

## Molecular Modeling of the Tributyl Phosphate Complex of Europium Nitrate in the Clay Hectorite

Cynthia J. Hartzell\*

Department of Chemistry, Northern Arizona University, Flagstaff, Arizona 86011-5698

Randall T. Cygan

Geochemistry Department, Sandia National Laboratories, Albuquerque, New Mexico 87185-0750

Kathryn L. Nagy

Department of Geological Sciences, University of Colorado, Boulder, Colorado 80309-0399

Received: February 11, 1998; In Final Form: June 17, 1998

Molecular modeling of the large tributyl phosphate complex of europium provides a test of the sensitivity of force field calculations to molecules within the interlayer of a trioctahedral smectite clay. A nonbonded version of the consistent-valence force field was utilized. Parametrization is based on the structures of simple clays and oxides. The simulations were carried out with complete translational freedom for all atoms. Energy minimization of the hectorite supercell containing, within the interlayer, the Eu·3TBP complex as the trinitrate, eight sodium cations, and 48 waters of hydration resulted in a  $d$  spacing of 18.66 Å. Molecular dynamics simulations at 298 K resulted in a  $d$  spacing of  $17.40 \pm 0.15$  Å. The experimental  $d$  spacing for hectorite absorbed with the TBP solvate of  $\text{Eu}(\text{NO}_3)_3$  is  $17.18 \pm 0.04$  Å.

### Introduction

Knowledge of the behavior of lanthanide and actinide organic complexes in the interlayer of clays is fundamental to predictive models for remediation of hazardous waste sites. Recent experimental evidence sheds light on the behavior in the clay hectorite of the neutral ligating agent tributyl phosphate (TBP) in complexation with the lanthanide europium.<sup>1</sup> Accurate molecular modeling of this large molecular system affords a powerful tool capable of visualization and prediction.

An extensive literature exists on the modeling of minerals and silicate phases. Molecular dynamics (MD) studies using optimized interatomic potentials<sup>2–4</sup> are successful in reproducing known structural and physical properties of silicate minerals. A recent monograph<sup>5</sup> covers work on the nature of the SiO bond and the interatomic potentials for Si, Al, and Mg oxides and Ca and Mg carbonates. Recently, investigators have gone on to apply first-principles MD to the study of various minerals.<sup>6,7</sup>

Successful applications of molecular mechanics to simulating the chemistry within the clay interlayer are best represented by studies of hydrated cations within smectites.<sup>8–12</sup> Studies of organic molecules within smectite clays are appearing in the literature.<sup>13</sup> Skipper et al.<sup>9,10</sup> successfully applied Monte Carlo calculations to the monolayer hydrates of Wyoming montmorillonite and vermiculite, verifying the results with comparisons to experimental data. In detailed studies, Chang et al.<sup>11,12</sup> obtained reasonable response of clay-layer  $d$  spacing to an increase in water monolayers within the montmorillonite interlayer using Monte Carlo techniques. Teppen et al.<sup>13</sup> have reported a MD simulation of the hexadecyltrimethylammonium ion in the dioctahedral smectite beidellite.

The force field methodology used in the present work has been applied successfully by Cygan et al.<sup>14</sup> to model the structure of kaolinite. That study represents a fully relaxed

structural analysis. The present study deals with an interlayer of a clay that is occupied not only by hydrated cations but also by a neutral organic ligate. Molecular mechanics calculations are carried out on the bulky europium–tributyl phosphate complex positioned within the interlayer of the clay hectorite, a magnesium–lithium silicate with sodium interlayer cations. An exhaustive simulation of this system must include counterions and water molecules within the interlayer. The success of this modeling problem requires accurate interatomic potentials not only for the waters of hydration and the counterions but also for the clay, the lanthanide cation, and the neutral organic ligand. Minimization and dynamics algorithms were called upon to handle a chemical system as large as 967 atoms. Measuring the success of these calculations requires experimental data that confirms the nature of the TBP species within the interlayer and the  $d$  spacing for the various absorbed and exchanged clays.

<sup>31</sup>P NMR studies confirmed that the tributyl phosphate (TBP) complex of europium, Eu·3TBP, is absorbed, intact, into the clay hectorite.<sup>1</sup> These studies also show that sequential addition of first europium and then TBP to the clay does not result in complex formation. Tributyl phosphate is commonly used as a ligating agent in the PUREX process for nuclear fuel processing and is a widespread contaminant in groundwater and soils<sup>15</sup> surrounding processing facilities. While the europium isotopes 151, 152, and 154 are present as contaminants in controlled releases, this study focuses on europium as an analogue for the behavior of high-level actinide contaminants. Previous studies<sup>16</sup> of the nature of the species formed upon uptake of europium nitrate into solvent TBP showed that the complex exists as the neutral, un-ionized nitrate solvated by a specific number of TBP molecules. This lanthanide complex

**TABLE 1: Potential Types and Charges Applied to Each Atom. Empirical Parameters,  $A_i$  and  $B_i$ , for the Lennard-Jones Potential**

interlayer species		type	charge	$A_i$ ((kcal/mol) $\text{\AA}^{12}$ ) $^{1/2}$	$B_i$ ((kcal/mol) $\text{\AA}^6$ ) $^{1/2}$
Na water:		Na ion in water	1	12 250.7	75.163
	H	H in water	0.41	$1.0 \times 10^{-8}$	0.00
	O	O in water	-0.82	629 358	625.50
Eu TBP:		calcium ion	3	119 025	240.25
	C	sp <sup>3</sup> carbons	-0.05 to -0.3	1 790 340	528.48
	H	H bonded to carbon	0.1	7108.46	32.871
	P	phosphorus	1.9	6 025 894	2195.60
	O	sp <sup>3</sup> oxygen in ether or ester	-0.50	272 895	498.88
	=O	O in carbonyl	-0.85	272 895	498.88
nitrate:	N	sp <sup>2</sup> nitrogen in nitro group	0.505	2 266 872	1230.56
	O	O in charged carboxylate	-0.168	272 895	498.88
			-0.668		
			-0.668		
hectorite	Mg	octahedral Mg ion in clays	2	27 194.4	2377.5
	Si	tetrahedral Si atom in clays	4	368.51	0.001 18
	O	oxygen atom in clays	-2	989 199	676.86
	Li	lithium ion with oxygen in clays	1	1154.3	0.000
	H	H in hydroxyl group in clays	1	0.0046	0.000

in TBP is unhydrated, in contrast to transition metal complexes that tend to be hydrated.

Solid-state NMR is a powerful technique for elucidating the details of ion siting in clays. Studies reported since 1990 of nuclei that are directly observable by the NMR analysis of clays include Cs<sup>+</sup> siting in hectorite,<sup>17</sup> kaolinite, and montmorillonite,<sup>18,19</sup> the behavior of Na<sup>+</sup>, Cd<sup>+</sup>, and Cs<sup>+</sup> in micas,<sup>20</sup> K<sup>+</sup> in smectites,<sup>21</sup> Na<sup>+</sup> in synthetic beidellite,<sup>22</sup> and Cd<sup>+</sup> in exchanged clays.<sup>23</sup> The lanthanide Eu is not directly observable by NMR. However, the dramatic effect of Eu on the NMR chemical shift of a neighboring atom provides a powerful probe of the proximity of Eu to complexing ligands. The <sup>31</sup>P MAS NMR studies<sup>1</sup> of the Eu/TBP system exploit this phenomenon to distinguish TBP in the free form from TBP as the complex Eu·3TBP. The <sup>31</sup>P signal of free TBP has a chemical shift of -0.7 ppm, while the <sup>31</sup>P signal of complexed TBP is shifted to -189 ppm.

### Computational and Experimental Methods

**Hectorite Simulation Cell.** The models for this study consisted of a standard 2:1 smectite structure. Hectorite is a Li-rich trioctahedral smectite clay with unit formula Na<sub>x</sub>(Mg<sub>0.88</sub>-Li<sub>0.12</sub>)Si<sub>4</sub>O<sub>10</sub>(OH)<sub>2</sub>·*n*H<sub>2</sub>O. Although hectorite is seldom found in soils, it was chosen as a model smectite for NMR study due to the low iron content.

The simulation cell consists of a supercell of hectorite made up of 32 unit cells and having *P1* symmetry. The triclinic cell has one clay layer of a 2:1 smectite structure, 670 atoms in size. The initial cell height was 20.6 Å. The tetrahedral sheets are constructed of linked SiO<sub>4</sub> units that are 9 Si tetrahedra in width and 16 Si tetrahedra in length, 21.3 Å × 36.9 Å. The octahedral sheet differs from that of montmorillonite in that Al<sup>3+</sup> is replaced by Mg<sup>2+</sup> and Li<sup>+</sup> yielding a trioctahedral structure. The net negative charge on the clay layers in the simulation cell arises from eight lithiums distributed in the octahedral sheet. This differs from a real clay, in which the distribution of charge is not regular. An overall neutral cell is obtained by adding hydrated Na<sup>+</sup> ions to the interlayer. This cell was used for simulations involving Eu·3TBP. Energy minimizations and MD simulations were carried out with and without three nitrate counterions.

A smaller simulation cell was used in studies varying the identity of the interlayer cation and the extent of hydration. This smaller triclinic cell was constructed of eight unit cells, the

tetrahedral sheet measures 4 Si tetrahedra in width and 9 Si tetrahedra in length, 10.6 Å × 18.4 Å. The initial cell height was 13.8 Å.

**Calculations.** The energy minimization and MD studies were carried out using software programs from Molecular Simulations, Inc. Dynamics calculations were carried out with the program Discover 3.0. The software was run on a Silicon Graphics Indigo II workstation with a R8000 processor. The empirical force field used to describe the clay layer structure is a nonbonded version of the consistent-valence force field (CVFF) called CVFF<sub>aug</sub>. Parametrization of the force field is based on the structures of simple clays and oxide phases; valence bonds between atoms are not required. The parameters were derived for periodic assemblies and require full ionic charges.

Available parameters include those for the atoms of organic molecules, ions in zeolites and clays, and ions hydrated by water. Nonbond terms are of particular importance in describing the mutual interlayer interactions of water, cations, neutral organophosphate, and clay sheet. The nonbond interactions include short-range, van der Waals, and electrostatic interactions. The short-range and van der Waals interactions are described by a Lennard-Jones function,

$$E_{\text{pot}} = \frac{\sqrt{A_i A_j}}{r^{12}} - \frac{\sqrt{B_i B_j}}{r^6}$$

where  $E_{\text{pot}}$  is the potential energy in terms of the empirical parameters  $A_i$  and  $B_i$  for atom  $i$  and for atom  $j$ . The distance between atoms  $i$  and  $j$  is given by  $r$ . Minimization and dynamics studies were carried out using resident parameters in Discover 3.0. The values for parameters  $A$  and  $B$  are tabulated in Table 1. The Coulombic representation of the electrostatic interaction is given as

$$E_{\text{pot}} = \frac{q_i q_j}{\epsilon r_{ij}}$$

where  $\epsilon$  is the dielectric constant and  $q$  is the atomic charge.

Parameters for the Eu potential are not included in the MSI software. In the current study, the parameters chosen for the europium ion (ionic radius = 0.95 Å) were based on those for Ca<sup>2+</sup> (ionic radius = 0.99 Å) applying a 3+ charge. Varnek

and Wipff<sup>24</sup> successfully used this approximation to perform MD simulations of  $\text{Eu}^{3+}$ -organo complexes.

The energy minimization and MD calculations were run using three-dimensional periodic boundary conditions to extend the surface and eliminate edge sites. In this method, the simulation cell is replicated periodically in space so that molecules in a cell interact with each other and with the periodic image. In contrast to previous studies,<sup>9,11,25</sup> all atoms of the simulation cell are allowed to freely translate with no symmetry constraints. Problems caused by long-range Coulomb interactions among replicated cells are reduced by using the method of Ewald summations. Skipper et al.<sup>9</sup> successfully applied this combination of three-dimensional periodic boundary conditions and Ewald sums in their Monte Carlo simulations of hydrated clays.

MD calculations were run at a temperature of 298 K and a constant pressure of 1 bar. The van der Waals and Coulomb interactions are calculated separately, both using the method of Ewald sums. The chemical system was treated as an NPT ensemble and required a Verlet algorithm for the integration of Newton's equations of motion.<sup>26</sup> In these systems, the total energy stabilizes within 10–15 ps. Typical simulation times of 25–30 ps were used for each MD calculation. The high-frequency vibrations associated with OH bonds often require relatively short time steps. Time steps of 0.5 and 0.25 fs were suitable for most calculations, although it was necessary to drop to 0.1 fs steps for calculation of the largest molecular system.

Mean  $d$  spacings for the MD simulations were determined by averaging over the simulated structures in the region of constant energy. The mean  $d$  spacing is calculated using the reported cell parameters at each frame of the relevant region.

**Materials.** Materials were prepared as previously described.<sup>1</sup> The spray-dried hectorite was used as supplied by NL Industries. The cation exchange capacity is 100 mequiv/100 g. The tributyl phosphate and  $\text{Eu}(\text{NO}_3)_3 \cdot 6\text{H}_2\text{O}$  were used as supplied by Aldrich.

**Preparation of Hectorite Adsorbed with Eu-3TBP.** The 3:1 TBP/Eu solution was prepared by dissolving 0.457 g (1.02 mmol) of  $\text{Eu}(\text{NO}_3)_3 \cdot 6\text{H}_2\text{O}$  into a solution of 0.83 mL (3.06 mmol) of TBP in 10 mL of hexane. One gram of hectorite (1.00 mequiv) was stirred in this solution for 24 h and then centrifuged. The clay was washed three times with hexane and then air-dried. IR spectral bands,  $\text{cm}^{-1}$ : TBP (neat) 2956 (s), 2926 (s), 2863 (s), 2353 (w, br), 2336 (w, br), 1469 (m), 1434 (w), 1392 (m), 1385 (m), 1284 (s), 1060 (s), 1034 (s), 987 (s), 906 (m), 810 (m);  $\text{Eu} \cdot 3\text{TBP}(\text{NO}_3)_3$  (neat) 2963 (s), 2863 (s), 2600 (w), 2505 (w), 2350 (m), 2271 (s), 1767 (w), 1733 (w), 1617 (m), 1493 (s), 1470 (s), 1380 (m), 1290 (s), 1207 (s), 1057 (s), 1020 (s), 963 (s), 807 (w).

**Preparation of Europium-Exchanged Hectorite.** Europium-exchanged hectorite (Eu-hectorite) was prepared by stirring 0.4 g of hectorite in 527 mL of 1.77 mM  $\text{Eu}(\text{NO}_3)_3 \cdot 6\text{H}_2\text{O}$ , yielding a ratio of 2.8 mequiv  $\text{Eu}^{3+}$ /0.40 mequiv hectorite. The solution was adjusted to a constant ionic strength of 0.014 with  $\text{NaClO}_4$  and a pH of 5 with HCl. After 24 h of stirring, the clay was separated by gentle centrifugation, washed with distilled water, and dried under a stream of  $\text{N}_2$ .

**NMR.** <sup>31</sup>P MAS NMR spectra of TBP were acquired at 81 MHz on a Bruker CXP-200 wide-bore spectrometer, 4.7 T, using a Doty 5 mm MAS probe at spinning speeds of 2.2–2.5 kHz. A Bloch pulse sequence was used with a 15  $\mu\text{s}$  pulse at 220 W and a relaxation delay of 5 s. Spectra were acquired at a sweep width of 50 000 Hz and were accumulated as 8 K complex data points. Spectra are the result of 14 000 transients. Chemical

shifts are reported relative to an external reference of 85% orthophosphoric acid.

**FTIR.** Vibrational analysis was carried out on a Nicolet 800 SX FTIR spectrometer with a microscope attachment in transmission mode. A small amount of material was compressed between two NaCl IR windows. The sample of hectorite absorbed with  $\text{Eu} \cdot 3\text{TBP}$  contains about 0.2 mmol of the complex per gram of clay. This means that nitrate is present at 1.2 wt %, which is at the limit of the technique for detecting a minority component in a majority material.

**X-ray Analysis.** The  $d$  spacing is determined by powder X-ray diffraction using a Cu tube. The data were collected over the  $2\theta$  range 2–45° at a step size of 0.02° and a 5 s threshold per step using a Siemens D-500 X-ray diffractometer. All curves were fitted using Person VII or pseudo-Voigt functions. Each clay was prepared as a slurry in ethanol and sedimented on a “zero-background” quartz slide and then allowed to dry at 20% relative humidity. All samples were run at 20% relative humidity and 76 °F.

## Results and Discussion

**Hydrated Ions within the Hectorite Interlayer.** Calculations probing the response of the hectorite structure to the presence of interlayer cations and waters of hydration preceded simulations involving the TBP-europium complex. The smaller simulation cell used in these calculations is shown in Figure 1A. This figure shows the energy-minimized structure of hectorite containing three sodium ions and 18 waters in the interlayer. Experimental and simulated  $d$  spacings for all systems are tabulated in Table 2.

The experimental  $d$  spacing obtained for our Na-hectorite sample was measured at a relative humidity of 20%. At 20% humidity, Chipera et al.<sup>27</sup> measured hydration values of 3.5 and 6.5 molecules of water per Na ion in the smectite Na-SAz.<sup>28</sup> (The two values reflect a hysteresis in hydration versus dehydration.) Sato et al.<sup>29</sup> showed that Na-SAz<sup>128</sup> and beidellite clays form the one-layer hydrate in the relative humidity range 30–50%. Delville's<sup>30</sup> calculations using a model montmorillonite indicate that the average number of water molecules in the first hydration sphere of sodium is 5.68 waters per ion. We ran energy minimization studies on the Na-hectorite cell with four waters per sodium ion and with six waters per sodium ion. In one starting configuration, 12 waters were distributed about three sodium ions in the interlayer. X-ray diffraction simulation of this energy-optimized structure produced a  $d$  spacing of 11.83 Å for the (001) basal reflection. In the second starting configuration, 18 waters were placed in octahedral positions about the three sodium ions. The  $d$  spacing increased to 12.57 Å. This value exceeds the experimental  $d$  spacing of 11.25 Å.

These energy-minimized structures displayed  $d$  spacings that are sensitive to the degree of hydration. The change in hydration from four waters to six waters per sodium results in an increase in the simulation  $d$  spacing of 6.7%. This behavior is consistent with the experimental observations of Chipera et al.<sup>27</sup> on the smectites Na-SAz and Na-SWy.<sup>28</sup> These clays show increases in  $d$  spacings of 15% as the water content of Na-SAz increases from 3.9 to 7.1 waters per gram of clay and 11% as the water content of Na-SWy increases from 4.1 to 6.5 waters per gram of clay.

A MD study of the hexahydrated Na ions in hectorite was carried out at 298 K for a total simulation time of 30 ps. A time step of 0.5 fs proved sufficient to maintain numerical stability. The system equilibrated within the first 10 ps. The



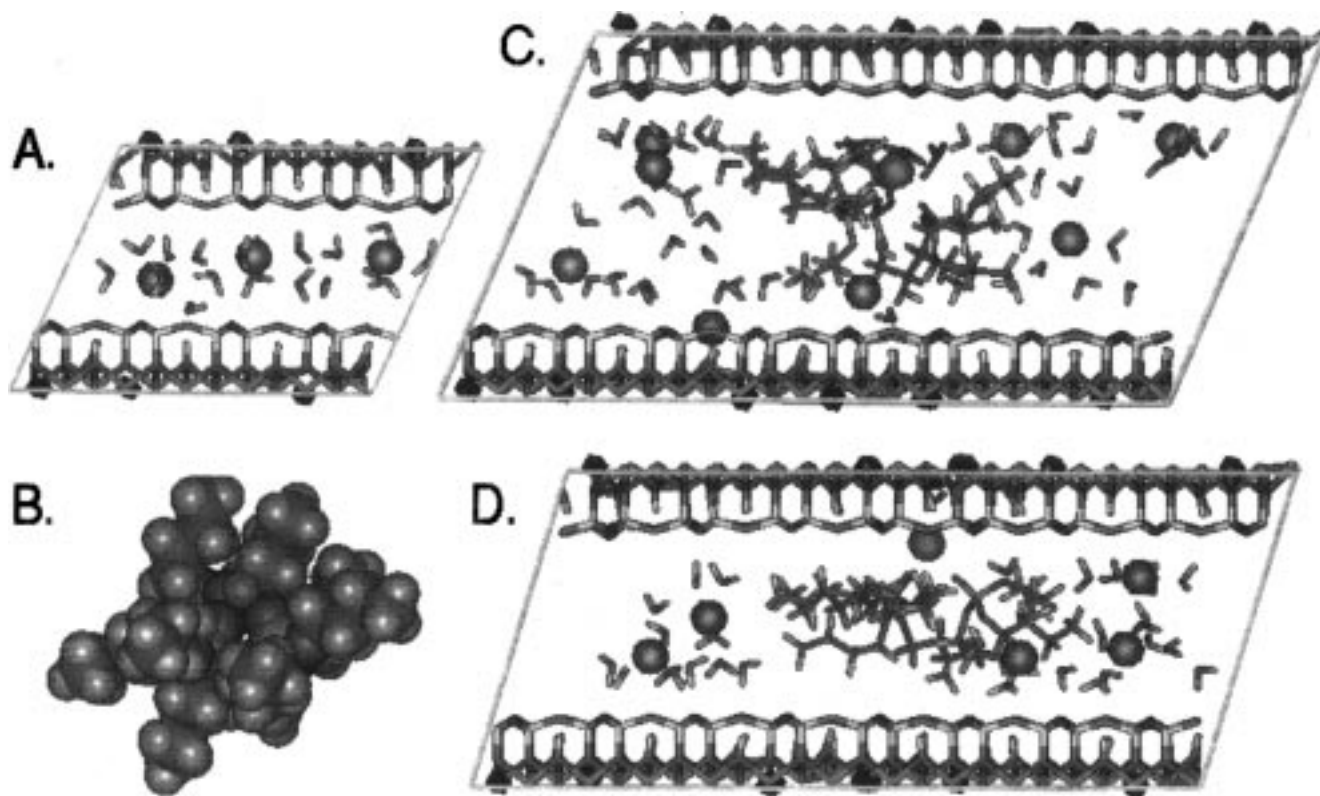


**Figure 1.** (A) Energy-minimized structure of hectorite containing three sodium ions and 18 waters in the interlayer of the small simulation cell. Hectorite is a magnesium–lithium silicate with sodium interlayer cations (Na = purple). The tetrahedral sheets are constructed of linked  $\text{SiO}_4$  units (Si = yellow, O = red). The octahedral sheet differs from that in montmorillonite in that  $\text{Al}^{3+}$  is replaced by  $\text{Mg}^{2+}$  and  $\text{Li}^+$  (Mg = lime green, Li = dark purple). (B) The energy-minimized structure of  $\text{Eu}^{3+}$  complexed with three tributyl phosphate molecules (Eu = light blue, P = pink, C = green, O = red, H = white). (C) Energy-minimized structure of system 1: the large hectorite simulation cell with the interlayer loaded with  $\text{Eu}\cdot 3\text{TBP}$  trinitrate, eight  $\text{Na}^+$  ions, and 48 waters (colors are the same as those in A and B plus N = dark blue). (D) Energy-minimized structure of system 2: the large hectorite simulation cell with the interlayer loaded with  $\text{Eu}\cdot 3\text{TBP}$ , five  $\text{Na}^+$  ions, and 30 waters (colors are the same as those in A and B).

**TABLE 2:  $d$  Spacings ( $\text{\AA}$ ) from Energy Minimization and MD Simulation of Hectorite with Specified Interlayer Occupancy. Experimental (XRD)  $d$  spacings from Relevant Samples Are Given**

hectorite interlayer	$d_{\text{min}}$	$d_{\text{MD}}$	$d_{\text{XRD}}$
hydrated ions			
$\text{Na}^+\cdot 4\text{H}_2\text{O}$	11.83	$11.74 \pm 0.12$	11.25
$\text{Na}^+\cdot 6\text{H}_2\text{O}$	12.57	$11.99 \pm 0.10$	11.25
$\text{Eu}^{3+}\cdot 6\text{H}_2\text{O}$	11.73	$11.05 \pm 0.08$	13.97
$\text{Eu}^{3+}\cdot 23\text{H}_2\text{O}$	13.89	$13.96 \pm 0.11$	13.97
complex			
$\text{Eu}^{3+}\cdot 3\text{TBP}$	16.09	$15.20 \pm 0.15$	17.18
$5\text{Na}^+\cdot 30\text{H}_2\text{O}$			
$\text{Eu}^{3+}\cdot 3\text{TBP}\cdot 3(\text{NO}_3^-)$	18.66	$17.40 \pm 0.15$	17.18
$8\text{Na}^+\cdot 48\text{H}_2\text{O}$			
$\text{Eu}^{3+}\cdot 3\text{TBP}\cdot 3(\text{NO}_3^-)$	19.12	$19.11 \pm 0.32$	17.18

mean basal  $d$  spacing is  $11.99 \pm 0.10 \text{ \AA}$ . The variation of  $d$  spacing over time is shown in Figure 2. The thermal “breathing” of the clay is demonstrated by the oscillation in  $d$  spacing. The average value is smaller than the value of  $12.57 \text{ \AA}$  obtained from the 0 K minimization. The MD study of hectorite with four waters per ion yielded a  $d$  spacing of  $11.74 \pm 0.12 \text{ \AA}$ , which is slightly smaller than the value of  $11.83 \text{ \AA}$  obtained from the 0 K minimization. The MD result for the four waters per ion most closely approaches the experimental  $d$  spacing of  $11.25 \text{ \AA}$ .

The average cell resulting from the MD simulation of hectorite with four waters per sodium has unit cell parameters  $a = 5.23 \text{ \AA}$ ,  $b = 9.08 \text{ \AA}$ ,  $c = 13.75 \text{ \AA}$ ,  $\alpha = 119.3^\circ$ ,  $\beta = 98.9^\circ$ , and  $\gamma = 90.0^\circ$ . Published experimental values<sup>31</sup> for the unit cell of Na–hectorite are  $a = 5.25 \text{ \AA}$  and  $b = 9.09 \text{ \AA}$ .

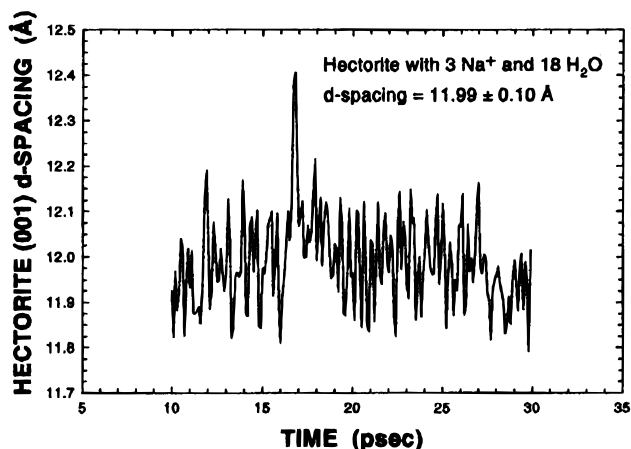


**Figure 2.** Variation of  $d$  spacing with time during the MD simulation of three hexahydrated Na ions in hectorite.

It is interesting to note the sensitivity of the calculation to the Na force field potential. The potential used in the previously described calculations was parametrized based on a hydrated Na ion. Changing this potential to a value derived from an unhydrated Na ion yields a  $d$  spacing of  $13.24 \text{ \AA}$  for the energy-minimized clay with hexahydrated Na ions, an increase of 5%. The use of Mg, O, Si, and H potentials optimized for the simulation of zeolites results in a  $d$  spacing of  $14.18 \text{ \AA}$  for the energy-minimized clay with hexahydrated Na ions, an increase of 13%.

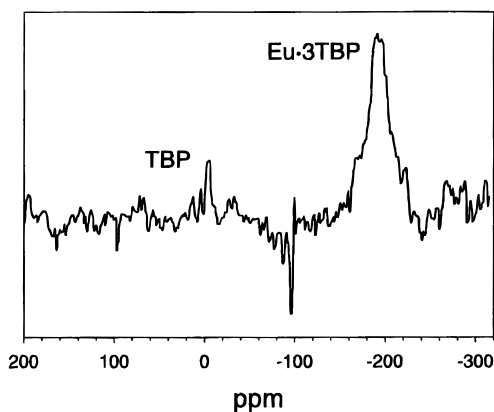


Figure 3.  $^{31}\text{P}$  MAS NMR spectrum of hectorite containing  $\text{Eu}\cdot 3\text{TBP}$ .

Energy minimizations were carried out on hectorite with an interlayer containing  $\text{Eu}^{3+}$  as the hexahydrate and as a hydrate with an excess of waters, 23 waters per ion. As in the case of sodium, the  $d$  spacing responds to the degree of hydration, yielding a value of 11.73 Å for the hexahydrate and a value of 13.89 Å for the state of excess hydration, an increase of 18%. The experimental  $d$  spacing measured on Eu-exchanged hectorite at 20% relative humidity is 13.97 Å. The MD simulation of the 23-water hydrate resulted in essentially no change in the  $d$  spacing, yielding an average value of  $13.96 \pm 0.11$  Å.

**Europium–Tributyl Phosphate Complexes within the Hectorite Interlayer.**  $^{31}\text{P}$  NMR experiments<sup>1</sup> confirmed that  $\text{Eu}^{3+}$  and TBP remain associated as the complex  $\text{Eu}\cdot 3\text{TBP}$  upon absorption from hexane into hectorite. The  $^{31}\text{P}$  MAS NMR spectrum of hectorite containing  $\text{Eu}\cdot 3\text{TBP}$  is shown in Figure 3. The phosphorus signal of the complex is shifted to  $-189$  ppm. The NMR study does not clarify whether this complex moves into the clay as the neutral trinitrate or as the positively charged species, which would leave the negative nitrate groups in the supernatant and displace  $\text{Na}^+$  from the interlayer. Previous studies<sup>16</sup> of the nature of the species formed upon uptake of lanthanides into solvent TBP showed that the complex exists as the neutral, unhydrated nitrate solvated by a specific number of TBP molecules.

The minimized structure of  $\text{Eu}^{3+}$  complexed with three neutral TBP molecules is shown in Figure 1B. Notice that the TBP molecules form a hydrophobic cap around the europium ion, exposing one surface for further complexation. The minimized structure of  $\text{Eu}\cdot 3\text{TBP}$  as the trinitrate is shown in Figure 4.

Simulations were carried out with the  $\text{Eu}\cdot 3\text{TBP}$  complex both as the neutral trinitrate and as the charged species. Specifically, simulations were carried out on (1) the large hectorite simulation cell with the interlayer loaded with  $\text{Eu}\cdot 3\text{TBP}$  trinitrate and eight hexahydrated Na ions and (2) the large hectorite simulation cell with the interlayer loaded with  $\text{Eu}\cdot 3\text{TBP}$  as the 3+ complex plus five hexahydrated Na ions. The minimized structures of systems 1 and 2 are shown in Figure 1C and 1D, respectively. The basal  $d$  spacing for the energy minimization of structures 1 and 2 are 18.66 and 16.09 Å, respectively. The experimental  $d$  spacing of hectorite absorbed with  $\text{Eu}\cdot 3\text{TBP}$  is  $17.18 \pm 0.04$  Å.

MD studies of these systems were carried out at 298 K for total simulation times of 25 ps. Time steps of 0.1 fs were necessary to complete the study of system 1. Time steps of 0.5 and 0.2 fs resulted in unrealistic excursions of a hydrogen from a water molecule. Time steps of 0.25 fs proved sufficient to carry the MD run on system 2 into a region of constant energy. Time steps of 0.5 and 0.33 fs resulted in unrealistic H

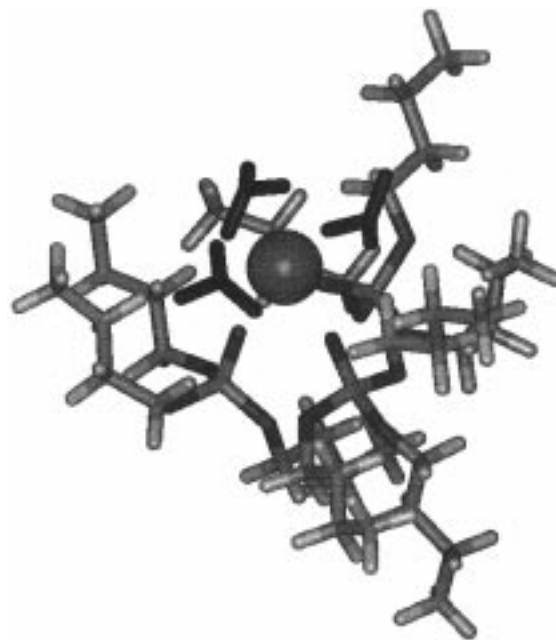


Figure 4. Energy-minimized structure of  $\text{Eu}(\text{NO}_3)_3\cdot 3\text{TBP}$ . The three nitrate groups, shown in black, sit above the Eu ion.

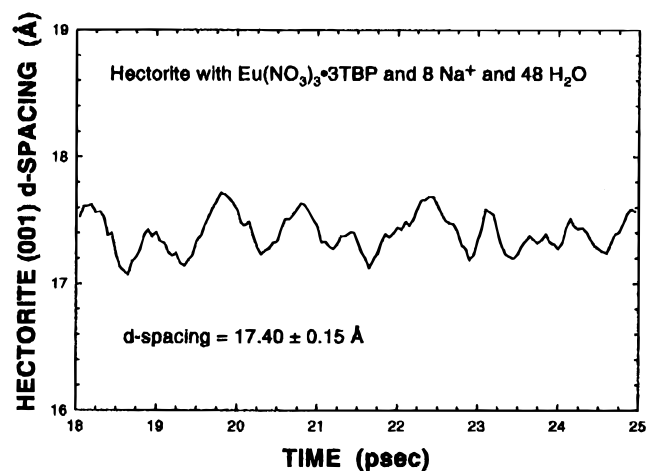


Figure 5. Variation of  $d$  spacing with time during the MD simulation of system 1.

excursions into the hectorite structure. These proton excursions in the MD runs are reminiscent of Delville's<sup>30</sup> observation that a water molecule above the hexagonal cavity of the siloxane layer can form a hydrogen bond with the lone pair of the oxygen at the center of the cavity.

The results of the MD studies yielded an average  $d$  spacing for system 1 of  $17.40 \pm 0.15$  Å, a decrease of 7% from the 0 K minimization. The variation of  $d$  spacing with time is shown in Figure 5. System 2 displays an average  $d$  spacing of  $15.20 \pm 0.15$  Å, a drop of 6% from the 0 K minimization. The MD  $d$  spacing for system 1 closely approaches the experimental  $d$  spacing of  $17.18 \pm 0.04$  Å, while the  $d$  spacing of system 2 is smaller by 2 Å. This argues for the presence in the interlayer of  $\text{Eu}\cdot 3\text{TBP}$  as the trinitrate.

FTIR studies are consistent with the presence of nitrate in the  $\text{Eu}\cdot 3\text{TBP}$ -absorbed clay. The overlay comparing the FTIR spectra of hectorite, neat TBP, TBP-absorbed hectorite, and  $\text{Eu}\cdot 3\text{TBP}$ -absorbed hectorite is shown in Figure 6. The spectrum of  $\text{Eu}\cdot 3\text{TBP}$ -absorbed hectorite displays a broad peak at  $1346\text{ cm}^{-1}$ , which is not present in the spectrum of TBP-absorbed hectorite. This peak is attributable to the  $\nu_3$  stretching mode

TABLE 3: Interatomic Distances from Energy Minimization and MD Simulations (Å)

	PO...Eu min	PO...Eu MD	NO...Eu min	NO...Eu MD	Na...OSi min	Na...OSi MD, av	SiO...Eu min	SiO...Eu MD, av
Gas Phase								
Eu·3TBP	2.22							
	2.22							
	2.22							
Eu·3TBP (NO <sub>3</sub> ) <sub>3</sub>	2.22	2.16	2.25	2.16				
	2.23	2.18	2.27	2.21				
	2.25	2.23	3.80	3.71				
			2.24	2.17				
			2.29	2.25				
			3.64	3.69				
			2.25	2.15				
			2.29	2.19				
			3.69	3.63				
Ions in Hectorite								
3 Na <sup>+</sup> , 18 H <sub>2</sub> O					2.48	2.61		
					2.50	2.74		
					2.53	2.43		
Eu <sup>3+</sup> , 23 H <sub>2</sub> O							3.66	3.66
Complex in Hectorite								
Eu <sup>3+</sup>	2.24	2.26				4.51	2.43	2.21
·3TBP,	2.25	2.28				4.53	2.61	2.51
5Na <sup>+</sup> ,	2.29	2.28				4.85	2.78	2.56
30 H <sub>2</sub> O						5.70		2.56
						7.81		2.70
								2.73
Eu·3TBP	2.23	2.22	2.24	2.28		2.35*		
(NO <sub>3</sub> ) <sub>3</sub> ,	2.24	2.23	2.37	2.30		2.55*		
8 Na <sup>+</sup> ,	2.24	2.24	3.83	3.90		2.63*		
48 H <sub>2</sub> O			2.24	2.24		4.18*		
			2.29	2.35		*Eu side		
			3.77	3.76		2.45		
			2.25	2.25		2.35		
			2.29	2.34		4.03		
			3.80	3.83		4.04		

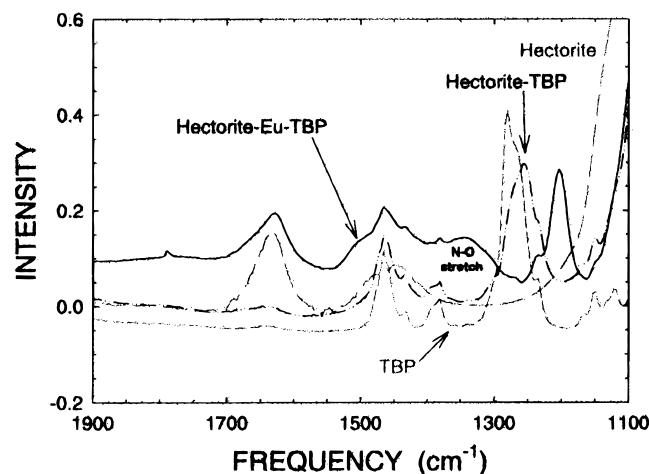


Figure 6. Comparison of the FTIR spectra of hectorite alone, TBP alone, TBP-adsorbed hectorite, and Eu·3TBP-adsorbed hectorite.

of the nitrate ion.<sup>32</sup> The IR spectrum (see Experimental Section) of neat Eu·3TBP displays strong bands at 1290 and 1493 cm<sup>-1</sup>. Such splitting has been characterized in crystalline nitrate-amine complexes and is attributed to splitting of the  $\nu_3$  mode in bidentate-coordinated nitrate.<sup>32</sup> The absence of these bands in the spectrum of the Eu·3TBP-adsorbed clay indicates an ionic nitrate, reflecting some dissociation of the nitrate ion. This was observed for the nitrate-amine complexes when dissolved in methanol.<sup>32</sup> The results of MD simulations on the gas-phase trinitrate Eu·3TBP complex and on system 1 (Table 3) are consistent with this observation. The interatomic distances between Eu and the two closest oxygens of each nitrate group

are larger by 5% in the clay-absorbed species, which may reflect greater ionic character. The average nitrate oxygen-to-Eu distances in the gas-phase MD simulations are 2.16 and 2.22 Å, while the comparable values for the clay-absorbed complex are 2.26 and 2.33 Å. Note that the two closest oxygens of each nitrate do not show identical distances.

Another striking feature of the IR spectra is the shift of the P=O stretch from 1284 cm<sup>-1</sup> in neat TBP to 1257 cm<sup>-1</sup> in the TBP-hectorite to 1208 cm<sup>-1</sup> in the clay-absorbed Eu·3TBP complex. This effect is well-known from the Raman spectra of phosphate glasses and crystalline compounds and is due to a decrease in the order of the phosphonyl bond when the oxygen coordinates with a cation.

The ability of the interlayer to accommodate the large Eu·3TBP complex can be visualized by viewing systems 1 and 2 from above the cell. In Figure 7, the average structures resulting from MD calculations on systems 1 and 2 are shown from above. The butyl arms of the three TBPs are seen to spread out in the plane of the interlayer like the spokes of a wheel.

Critical interatomic distances from the minimization and MD studies are tabulated in Table 3. For both system 1 and system 2, the Eu-to-phosphate oxygen distances in minimization and MD results differ by only 1.3%. A comparison of Figure 1C and 1D shows that the europium placement differs dramatically in the optimized structures for systems 1 and 2. The average structure for system 1 surrounds the europium with TBP and nitrates, placing europium about 4 Å from the siloxane oxygens. In contrast, the average MD structure for system 2 centers the Eu<sup>3+</sup> over a siloxane ring at distances ranging from 2.51 to 2.70



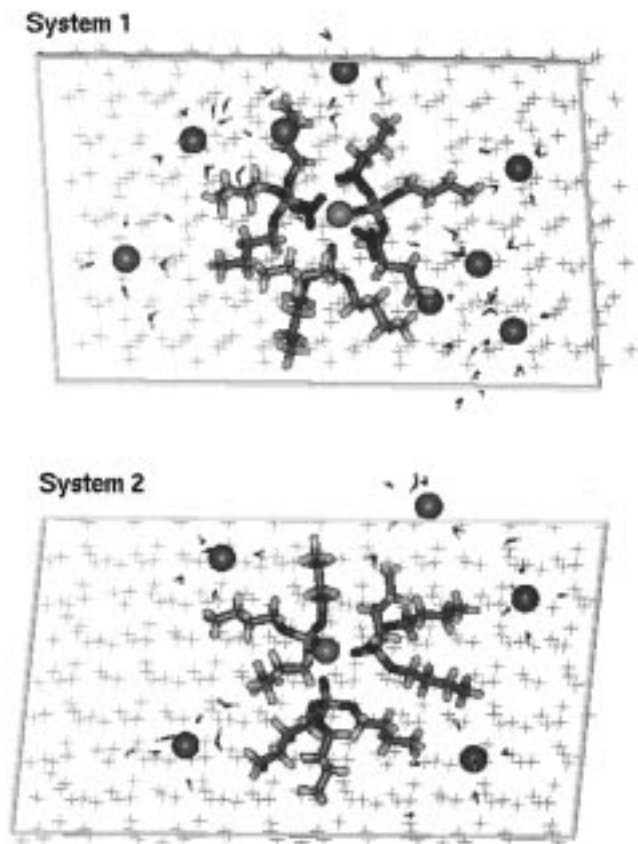


**Figure 7.** Average structures resulting from the MD simulations of systems 1 and 2 as viewed from above.

Å from the closest four siloxane oxygens and sitting 2.21 Å over a lower level oxygen.

The complexation sphere differs for the two systems. In the MD results on system 1, the nitrates orient toward the europium as in a bidentate structure with the six oxygens at an average distance of 2.29 Å. (Energy minimization yields 2.28 Å.) The average distance between  $\text{Eu}^{3+}$  and the P=O oxygens of TBP measures 2.23 Å. In system 2, the average distance between the P=O oxygens and  $\text{Eu}^{3+}$  measures 2.27 Å, and the average distance from  $\text{Eu}^{3+}$  to the closest six siloxane oxygens is 2.54 Å. Thus, the complexation distances in the trinitrate are shorter than in the charged complex.

The sodium ions display vastly different behavior in the MD results of the two systems. The distances from Na to the nearest siloxane surface are given in Table 3. In system 1, the sodium ions gravitate toward the charged layers, with five ions sitting 2.35–2.63 Å from the nearest sheet while three ions are 4.03–4.18 Å from the nearest sheet. In the case of system 2, the sodium ions tend to be centered within the interlayer at an average distance of 5.48 Å from the siloxane oxygens. These structures are consistent with the fact that the nitrates shield  $\text{Eu}^{3+}$  from the negative layer charge. The sodium ions, then, are attracted to the residual charge on the clay layers. In the absence of the nitrates, the  $\text{Eu}^{3+}$  interacts closely with the negative layer charge, leaving the layers less attractive to the sodium ions.

The response of minimizations to the removal of sodium ions from the interlayer is consistent with the analysis by Delville<sup>30</sup> based on Monte Carlo simulations. When sodium ions and water are removed from the hectorite interlayer leaving only the trinitrate  $\text{Eu}\cdot 3\text{TBP}$  complex, the simulated  $d$  spacing actually increases to 19.11 Å, an increase of 10%. Delville argued that

the electrostatic repulsion between the negatively charged clay layers is countered by the presence of the positive counterions, resulting in a system that is neutral and attractive.

**Gas-Phase Minimizations of TBP and  $\text{Eu}\cdot 3\text{TBP}$ .** Energy minimizations of TBP in the gas phase have verified the existence of a minimum energy configuration for two TBP molecules in proximity to each other. Beudaert et al.<sup>33</sup> have probed this behavior in detail in their theoretical study of TBP in water and in chloroform. For the two TBP molecules, the minimum structure places the two P=O oxygens at a distance of 5.74 Å. Energy minimization of three TBP molecules in proximity to  $\text{Eu}^{3+}$  yields a minimum structure with the P=O oxygens of TBP clustered about the cation at a distance of 2.22 Å, as shown in Figure 1B. The molecule is an oblate spheroid measuring 16.96 Å across the larger diameter and 11.39 Å across the shorter diameter.

Energy minimization of the  $\text{Eu}\cdot 3\text{TBP}$  structure with three nitrates yields a minimized structure with the six closest nitrate oxygens at an average position of 2.27 Å from the  $\text{Eu}^{3+}$ . The distances from the P=O oxygens to  $\text{Eu}^{3+}$  average 2.23 Å. The MD results yield average nitrate distances of 2.19 Å and a  $\text{PO}\cdots\text{Eu}$  average distance of 2.19 Å. It is interesting that these gas-phase MD values are significantly shorter than the distances obtained from the MD of the same complex within the clay: nitrate distances of 2.29 Å and  $\text{PO}\cdots\text{Eu}$  distances of 2.23 Å.

## Conclusions

Force field-based energy minimizations and MD studies have resulted in structures with  $d$  spacings that are within 4% of the experimental values. Optimized structures are sensitive to the number and type of counterions in the interlayer and to the degree of hydration. In addition, the simulation cells incorporating the TBP complex are sensitive to the charge of the complex. The molecular modeling software and computer workstation have handled properly a system approaching 1000 atoms. Simulations confirm that the clay hectorite is able to accommodate the bulky  $\text{Eu}\cdot 3\text{TBP}$  complex within the interlayer either as the charged complex or as the neutral trinitrate. This work serves to validate the use of force field calculations for predicting the behavior of lanthanide and actinide complexes in clays.

**Acknowledgment.** This work was supported by funding from the U.S. Department of Energy, Office of Basic Energy Sciences, Geosciences Research Program under contract DE-AC04-94AL85000 with Sandia National Laboratories (R.T.C., K.L.N.). C.J.H. acknowledges sabbatical support from Northern Arizona University.

## References and Notes

- (1) Hartzell, C. J.; Yang, S. W.; Parnell, R. A.; Morris, D. E. *J. Phys. Chem.* **1995**, *99*, 4205.
- (2) Catlow, C. R. A.; Price, G. D. *Nature* **1990**, *347*, 243.
- (3) Gale, J. D.; Cheetham, A. K. *Zeolites* **1992**, *12*, 674.
- (4) Kim, S.-C.; Keskar, A. V.; McCormick, A. V.; Chelikowsky, J. R.; Davis, H. T.; *J. Chem. Phys.* **1995**, *102*, 8656.
- (5) Silvi, B.; D'Arco, P., Eds. *Modelling of Minerals and Silicated Materials*; Kluwer Academic Publishers: Boston, 1997.
- (6) Wentzcovitch, R. M. First Principles Molecular Dynamics with Variable Cell Shape. In *Quantum Mechanical Theory of Real Materials*; Chelikowsky, J. R., Louie, S. G., Kluwer Acad. Pub.: Dordrecht, 1995.
- (7) Wentzcovitch, R. M.; Price, G. D.; High-Pressure Studies of Mantle Minerals by Ab Initio Variable Cell Shape Molecular Dynamics. In ref 5.
- (8) Skipper, N. T.; Refson, K.; McConnell, D. C. *J. Chem. Phys.* **1991**, *94*, 7434.
- (9) Skipper, N. T.; Chang, F. C.; Sposito, G. *Clays Clay Miner.* **1995**, *43*, 285.

- (10) Skipper, N. T.; Sposito, G.; Chang, F. C. *Clays Clay Miner.* **1995**, *43*, 294.
- (11) Chang, F. C.; Skipper, N. T.; Sposito, G. *Langmuir* **1995**, *11*, 2734.
- (12) Chang, F. C.; Skipper, N. T.; Sposito, G. *Langmuir* **1998**, *14*, 1201.
- (13) Teppen, B. J.; Rasmussen, K.; Bertsch, P. M.; Miller, D. M.; Schafer, L. *J. Phys. Chem. B* **1997**, *101*, 1579.
- (14) Cygan, R. T.; Hobbs, J. D.; Nagy, K. L. *Theoretical Models of Kaolinite: Bulk and Surface Structures*; 1997 International Clay Conference, Abstracts, 11, A18.
- (15) Riley, R. G.; Zachara, J. M. *Chemical Contaminants on DOE Lands and Selection of Contaminant Mixture for Subsurface Science Research*; DOE/ER-05477; U.S. Department of Energy: Office of Energy Research, Washington, DC, 1992.
- (16) Healy, T. V.; McKay, H. A. C. *Trans. Faraday Soc.* **1956**, *52*, 633.
- (17) Weiss, C. A. Jr.; Kirkpatrick R. J.; Altaner S. P. *Geochim. Cosmochim. Acta* **1990**, *54*, 1655.
- (18) Weiss, C. A., Jr.; Kirkpatrick R. J.; Altaner S. P. *Am. Mineral.* **1990**, *75*, 970.
- (19) Kim, Y.; Cygan, R. T.; Kirkpatrick, R. J. *Geochim. Cosmochim. Acta* **1996**, *60*, 1041.
- (20) Laperche, V.; Lambert, J. F.; Prost, R.; Fripiat, J. J. *J. Phys. Chem.* **1990**, *94*, 8821.
- (21) Lambert, J. F.; Prost, R.; Smith, M. E. *Clays Clay Mineral.* **1992**, *40*, 253.
- (22) Klopogge, J. T.; Jansen, J. B. H.; Schuiling, R. D.; Geus, J. W. *Clays Clay Mineral.* **1992**, *40*, 561–566.
- (23) Tinet, D.; Faugere, A. M.; Prost, R. *J. Phys. Chem.* **1991**, *95*, 8804.
- (24) Varnek, A.; Wipff, G. *J. Phys. Chem.* **1993**, *97*, 10840.
- (25) Karaborni, S.; Smit, B.; Heidug, W.; Urai, J.; van Oort, E. *Science* **1996**, *271*, 1102.
- (26) Frenkel, D.; Smit, B. *Understanding Molecular Simulation*; Academic Press: San Diego, 1996; pp 1–443.
- (27) Chipera, S.; Bish, D.; Carey, W. Los Alamos National Laboratories, unpublished results, 1997.
- (28) This is a Clay Minerals Society Standard clay: see: Van Olphen, H.; Fripiat, J. J. *Data Handbook for Clay Materials and Other Non-Metallic Minerals*; Pergamon Press: New York, 1979; pp 1–346.
- (29) Sato, T.; Watanabe, T.; Otsuka, R. *Clays Clay Mineral.* **1992**, *40*, 103.
- (30) Delville, A. *Langmuir* **1991**, *7*, 547.
- (31) Kadi-Hanifi, M.; Mering, J. C. R. *Hebd. Seanc. Acad. Sci., Paris* **1972**, *274D*, 149.
- (32) Curtis, N. F.; Curtis, Y. M. *Inorg. Chem.* **1965**, *4*, 804.
- (33) Beudaert, P.; Lamare, V.; Dozol, J. F. *Solv. Extr. Ion Exch.* **1998**, *16*, 597.